2D IR spectra of cyanide in water investigated by molecular dynamics simulations

Lee, Myung Won ; Carr, Joshua K ; Göllner, Michael ; Hamm, Peter ; Meuwly, Markus

Abstract: Using classical molecular dynamics simulations, the 2D infrared (IR) spectroscopy of CN(-) solvated in D2O is investigated. Depending on the force field parametrizations, most of which are based on multipolar interactions for the CN(-) molecule, the frequency-frequency correlation function and observables computed from it differ. Most notably, models based on multipoles for CN(-) and TIP3P for water yield quantitatively correct results when compared with experiments. Furthermore, the recent finding that T1 times are sensitive to the van der Waals ranges on the CN(-) is confirmed in the present study. For the linear IR spectrum, the best model reproduces the full widths at half maximum almost quantitatively (13.0 cm(-1) vs. 14.9 cm(-1)) if the rotational contribution to the linewidth is included. Without the rotational contribution, the lines are too narrow by about a factor of two, which agrees with Raman and IR experiments. The computed and experimental tilt angles (or nodal slopes) as a function of the 2D IR waiting time compare favorably with the measured ones and the frequency fluctuation correlation function is invariably found to contain three time scales: a sub-ps, 1 ps, and one on the 10-ps time scale. These time scales are discussed in terms of the structural dynamics of the surrounding solvent and it is found that the longest time scale (10 ps) most likely corresponds to solvent exchange between the first and second solvation shell, in agreement with interpretations from nuclear magnetic resonance measurements.

DOI: https://doi.org/10.1063/1.4815969

2D IR spectra of cyanide in water investigated by molecular dynamics simulations

Myung Won Lee, Joshua K. Carr, Michael Göllner, Peter Hamm, and Markus Meuwly

Citation: The Journal of Chemical Physics **139**, 054506 (2013); doi: 10.1063/1.4815969
View online: http://dx.doi.org/10.1063/1.4815969
View Table of Contents: http://scitation.aip.org/content/aip/journal/jcp/139/5?ver=pdfcov
Published by the AIP Publishing

2D IR spectra of cyanide in water investigated by molecular dynamics simulations

Myung Won Lee,[1] Joshua K. Carr,[2] Michael Göllner,[1] Peter Hamm,[3,a)] and Markus Meuwly[1,b)]

[1]*Department of Chemistry, University of Basel, Klingelbergstrasse 80, CH-4056 Basel, Switzerland*
[2]*Department of Chemistry and Theoretical Chemistry Institute, University of Wisconsin, 1101 University Avenue, Madison, Wisconsin 53706, USA*
[3]*Institute of Physical Chemistry, University of Zurich, Winterthurerstrasse 190, CH-8057 Zurich, Switzerland*

(Received 29 May 2013; accepted 28 June 2013; published online 2 August 2013)

Using classical molecular dynamics simulations, the 2D infrared (IR) spectroscopy of CN^- solvated in D_2O is investigated. Depending on the force field parametrizations, most of which are based on multipolar interactions for the CN^- molecule, the frequency-frequency correlation function and observables computed from it differ. Most notably, models based on multipoles for CN^- and TIP3P for water yield quantitatively correct results when compared with experiments. Furthermore, the recent finding that T_1 times are sensitive to the van der Waals ranges on the CN^- is confirmed in the present study. For the linear IR spectrum, the best model reproduces the full widths at half maximum almost quantitatively (13.0 cm^{-1} vs. 14.9 cm^{-1}) if the rotational contribution to the linewidth is included. Without the rotational contribution, the lines are too narrow by about a factor of two, which agrees with Raman and IR experiments. The computed and experimental tilt angles (or nodal slopes) α as a function of the 2D IR waiting time compare favorably with the measured ones and the frequency fluctuation correlation function is invariably found to contain three time scales: a sub-ps, 1 ps, and one on the 10-ps time scale. These time scales are discussed in terms of the structural dynamics of the surrounding solvent and it is found that the longest time scale ($\approx$10 ps) most likely corresponds to solvent exchange between the first and second solvation shell, in agreement with interpretations from nuclear magnetic resonance measurements. © *2013 AIP Publishing LLC*. [http://dx.doi.org/10.1063/1.4815969]

I. INTRODUCTION

The dynamics of small solute molecules in solution provides detailed information on the coupling between intra- and intermolecular degrees of freedom. Many experimental methods have been devised to characterize the interactions between the solvent and solute. 2D infrared (IR) spectroscopy is one of these methods, and has been shown to be very sensitive to dynamics on short time scales. This provides the opportunity to validate atomistic computational models against detailed experimental data.

In 2D IR spectroscopy, multiple ultrafast IR laser pulses are used. From the shape and time evolution of the 2D IR spectrum, it is possible to investigate processes which are difficult to study with linear IR experiments, as conventional methods can only provide highly averaged information. 2D IR spectroscopy can simplify complex spectra composed of many overlapping peaks and thus enhance spectral resolution by spreading peaks into the second dimension. Although 2D IR spectroscopy cannot provide the structure of molecular systems at atomic resolution, its time resolution on the subpicosecond scale enables the direct observation of fast dynamical processes. For example, 2D IR spectroscopy can be used for the study of chemical exchange between solvent and solute molecules,[1,2] dynamics of extended hydrogen bonding networks of water,[3–21] structure determination of complex biological molecules,[22–24] and rotational isomerization of small molecules in solution.[25]

The dynamical behavior of the cyanide ion (CN^-) has been well studied experimentally,[26–28] and it was found that simulations can give energy relaxation times in good agreement with experiment.[29,30] From 2D IR spectroscopic measurements, it has been shown that cyanide undergoes spectral diffusion on ultrafast time scales.[28,31] It has been suggested that the spectral dephasing of the cyanide ion consists of a rapid inertial process in the homogeneous limit and an additional slower spectral diffusion process.[28] Here, we use molecular dynamics (MD) simulations, from which the linear and 2D IR spectroscopic signals can be computed and used to characterize and understand the properties of aqueous CN^-.

Extensive theoretical and computational studies have been carried out to understand in more detail the dynamical and structural properties that are probed by 2D IR spectroscopy.[32–40] The dynamics of the simulated system may depend sensitively on the force field used, which in turn will affect interpretations of the simulations. Our previous study on the vibrational relaxation of CN^- in water revealed that classical MD simulations can realistically describe relaxation behavior if the force field used in the simulations is carefully improved.[30] In particular, it was found that by employing multipolar electrostatics with fine-tuning of the van der Waals

a)Electronic mail: phamm@pci.uzh.ch
b)Electronic mail: m.meuwly@unibas.ch

ranges, a quantitatively correct analysis of vibrational relaxation can be achieved. Concomitantly, the pathway for energy relaxation, which is very difficult to study experimentally, can be determined from these simulations.

By using appropriate approximations, it is possible to obtain from 2D IR spectroscopic experiments the frequency fluctuation correlation function (FFCF), $C(t) = \langle \delta\omega(0)\delta\omega(t)\rangle$, where $\delta\omega(t)$ is the instantaneous deviation of the transition frequency from the mean of the sample of interest. FFCFs can also be obtained easily from MD simulations and therefore play an important role in relating experiment and computer simulations. From the frequency trajectory $\omega(t)$, 2D IR spectra can be computed using various procedures. Two approaches which are considered in the present work are the use of the cumulant approximation and a procedure avoiding the cumulant approximation. The observables computed from the MD simulations depend on the conformations sampled which, in turn, are affected by the force field used. Hence, comparison with experimental data is mandatory as it provides a sensitive means to validate atomistic force fields. In turn, once validated, simulations provide the potential to analyze quantities which are difficult or impossible to observe directly from experimental measurements.

In this work, we used MD simulations of solvated CN^- with a range of interaction models. Conformations and the frequencies of the cyanide ion including the solvent environment were computed from the same interaction model and then analyzed with established procedures. Comparison with experimental measurements[28] was then used to judge the validity of the models for the intermolecular interactions. This is subsequently discussed in view of previous investigations of the vibrational relaxation of cyanide in water. Finally, observations related to the underlying solvent dynamics of the system and to the possible atomistic and structural interpretations of the time scales observed are discussed.

II. COMPUTATIONAL METHODS

All MD simulations were carried out with the CHARMM program[41] with provisions for multipolar interactions.[42] The simulations were carried out with spherical boundary conditions (SBC) and one cyanide ion solvated inside a water sphere of radius 19 Å containing 997 heavy water molecules, with a water density close to 1.11 g/cm^3. First, a cyanide ion was placed in a cubic water box with edge length of 31 Å containing 997 heavy water molecules. Then, the system was optimized under a spherical potential, followed by heating to 300 K. The system was equilibrated for 120 ps, first in the canonical (constant temperature, NVT) ensemble, then in the microcanonical (constant energy, NVE), and finally again in the NVT ensemble. Then, production simulations with SBC in the NVT ensemble followed. A snapshot of the equilibrated system is shown in Figure 1. For the simulations in the NVT ensemble, a Nosé-Hoover thermostat was employed with a thermal piston mass $Q = 50$ kcal mol^{-1} ps^2.[43,44]

The stretching potential for the cyanide ion is a Morse potential

$$V(r) = D_e\{1 - \exp[-\beta(r - r_e)]\}^2, \qquad (1)$$

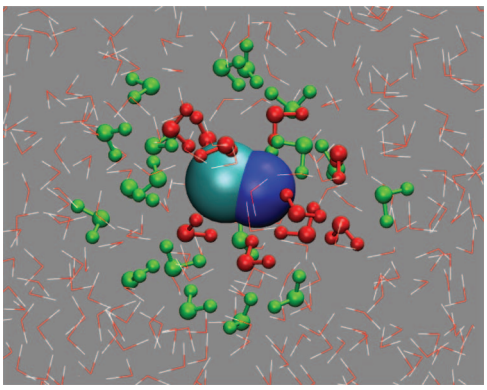

FIG. 1. The simulation system used in the present work. The C and N atoms of the cyanide ion are displayed as van der Waals spheres. The atoms of the water molecules whose oxygen atoms are within 4 Å (1st solvation shell) from the center of the cyanide ion are shown as red spheres and those between 4 and 6 Å (2nd solvation shell) as green spheres. Other water molecules are depicted as lines.

with parameters $D_e = 237.5$ kcal/mol, $\beta = 2.283$ Å^{-1}, and $r_e = 1.172$ Å.[45] The Lennard-Jones (LJ) parameters for the cyanide ion were those from the universal force field (UFF):[46] $\epsilon^C = 0.105$ kcal/mol, $\sigma^C = 1.9255$ Å, $\epsilon^N = 0.069$ kcal/mol, and $\sigma^N = 1.8300$ Å. For ϵ always the original UFF values were used, whereas for σ both original and scaled values were considered. In previous work, it was found that scaling $\sigma(= r_{min}/2)$ by +7.5 % almost quantitatively reproduces the experimental vibrational relaxation time of CN^- in H_2O.[30]

For the electrostatic interactions of cyanide, a multipolar (MTP), a 3-point charge model, and a conventional point charge model based on charges from electrostatic potentials using a grid based method (CHELPG)[47] were used. For the MTP, a distributed multipole analysis (DMA) is employed.[48] The multipole moments for CN^- are calculated from density functional theory (DFT) calculations at the B3LYP/aug-cc-pVQZ level. The GAUSSIAN 03 suite of programs[49] was used to obtain the SCF wavefunctions, from which the charges q and the components of the dipole $\vec{\mu}$ and quadrupole Θ on the C and N atoms were calculated through the GDMA program.[48] Each multipole moment Q was calculated on a grid ranging from 0.9 to $1.1 \cdot r_e$ with a step size of $0.01 \cdot r_e$, where $r_e = 1.177$ Å is the experimentally determined equilibrium bond length.[50] The values of all nonzero components up to quadrupole are summarized in Table I.[30] To describe the orientations of the atomic multipole moments with respect to the global Cartesian coordinate system, the reference axis system is assigned to the molecule, and the interactions are transformed at each step to the global axis system.[51] For the cyanide anion, the charge distribution is axially symmetric, and only one axis is required. Here, the z-axis is chosen, which is parallel to the molecular axis (see Table I).

For the 3-point charge model, which is computationally less expensive, we followed the procedures employed previously.[52–54] Here, charges are placed on the carbon and nitrogen atoms and an extra point charge is placed at the center of mass of the diatomic molecule in such a way that the charge, dipole moment, and quadrupole moment computed from the quantum calculations are reproduced. Cubic

TABLE I. Parameters of CN^- for (1) the multipole model and (2) the 3-point charge model. The reference data of CN^- were obtained from B3LYP/aug-cc-pVQZ around the equilibrium bond length. Each multipole component is denoted by Q_u, where u represents angular momentum labels (00, 10, 11c, 11s, 20, 21c, 21s, 22c, and 22s). The molecular axis is oriented along the z-axis, and only nonzero components are shown. For the 3-point charge model, charges on the C and N atoms are fitted to a function of the form $q = a_0 + a_1 r + a_2 r^2 + a_3 r^3$, where r is the bond distance of CN^-. The parameters of the fits are given in the last 4 columns.

Site	Q_{00} [e]	Q_{10} [ea_0]	Q_{20} [ea_0^2]	a_0 [e]	a_1 [eÅ^{-1}]	a_2 [eÅ^{-2}]	a_3 [eÅ^{-3}]
C	−0.447	0.973	0.318	−21.2	39.2	−26.4	6.2
N	−0.553	−0.698	0.963	−21.5	40.9	−28.2	6.8

functions, $q = a_0 + a_1 r + a_2 r^2 + a_3 r^3$, were fitted to the charges on the C and N atoms, where q is the charge, r is the bond distance of CN^-, and a_0 to a_3 are fitting parameters, reported in Table I. The same quantum calculations as for the DMA parameters described above were used as the reference data to which the 3-point charge model was fitted.

The electrostatic potential around the cyanide ion computed using the parameters of the 3-point charge model is compared with the potentials computed from the MTP parameters and from the SCF density of the DFT calculation in Figure 2. The potentials from various methods are quite similar outside ≈2.5 Å from the CN^-, but they differ close to the ion. The dipole and quadrupole moments of CN^- computed from the parameters of the 3-point charge model are 0.240 ea_0 and −3.65 ea_0^2, compared to 0.241 ea_0 and −3.66 ea_0^2 from MTP. To the best of our knowledge, no molecular gas-phase dipole and quadrupole moments have been reported so far.

For water, two different models are employed. One is a standard TIP3P potential[56] with or without SHAKE.[57,58] In addition, a flexible water model based on the parametrization by Kumagai, Kawamura, and Yokokawa[55] (KKY) is used with different charge models (*vide infra*). The time step in all simulations was $\Delta t = 0.4$ fs to account for the flexible O–H bonds in the KKY potential. The functional form of the KKY potential for the stretching and bending energies is

$$E_{\text{str}} = D\{1 - \exp[-\beta(r - r_0)]\}^2 \tag{2}$$

and

$$E_{\text{bend}} = 2 f_k \sqrt{k_1 k_2}\ \sin^2(\theta - \theta_0), \tag{3}$$

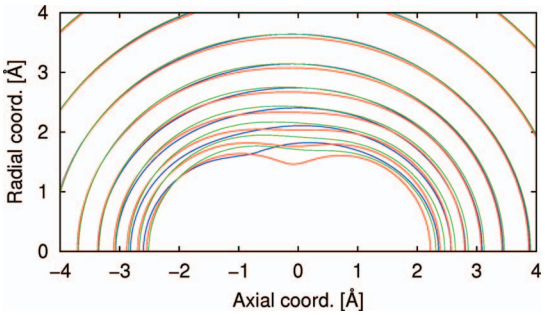

FIG. 2. Electrostatic potential obtained from the SCF density of the DFT calculation (blue), MTP parameters (red), and 3-point charge model parameters (green). The geometric center of CN^- is at the origin and the atoms are placed at zero radial coordinate. The C atom is along the negative axis and the N atom is along the positive axis.

where $k_i = 1/\{\exp[g_r(r_i - r_m)] + 1\}$, in which r_i is the distance of one O–H bond of the water molecule and g_r and r_m are parameters. All the KKY parameters used in the present work are summarized in Table II.[30] With KKY, electrostatic interactions are either TIP3P charges or multipole moments previously determined,[59] which are independent of the geometry of the water molecule. For the Lennard-Jones parameters σ and ϵ, those of the TIP3P model were used in all simulations. Because different force fields are used for both CN^- and H_2O, they can be combined in various ways which are all summarized in Table III. As explained further below, simulations with model M5 (M4 with modified van der Waals radii on the CN^- ion) were carried out in addition.

A. 2D IR spectra

Snapshots containing the coordinates of the cyanide anion and water molecules within 5.0 Å from the cyanide have been recorded every 10 steps (4 fs). Next, CN^- stretch frequencies were determined from $V(r)$ which was evaluated at the equilibrium bond length $r_e = 1.172$ Å and 6 additional points, including the classical turning points of the $v = 0$, 1, and 2 vibrational states, ranging from $r_{CN} = 1.069$ to 1.303 Å. This range of bond distance was selected as the vibrational transitions involved in the 2D IR spectra in this work are $0 \rightarrow 1$, and $1 \rightarrow 2$. The bond distance was changed so as to preserve the center of mass of the diatomic molecule. The energies were then fitted to a Morse potential. While the Morse potential has the same functional form as Eq. (1), the shape of the potential is perturbed due to the water molecules surrounding and interacting with the cyanide ion. The stationary states of the time-independent Schrödinger equation with the Morse potential can be evaluated analytically as

$$E_n = h\nu_0(n + 1/2) - \frac{[h\nu_0(n + 1/2)]^2}{4D_e}, \tag{4}$$

where $\nu_0 = (\beta/2\pi)\sqrt{2D_e/m}$ and m is the reduced mass of the cyanide ion. The frequency ω for the $(v = 0) \rightarrow (v = 1)$

TABLE II. Parameters for water potential reported in the work of Kumagai *et al.*[55] and used in this work. Atomic units are used for D, β, r_0, f_k, r_m, and g_r. θ_0 is given in degrees.

	D [E_h]	β [a_0^{-1}]	r_0 [a_0]	f_k [E_h]	θ_0 [deg]	r_m [a_0]	g_r [a_0^{-1}]
KKY	0.120	1.45	1.55	2.5×10^6	99.5	2.65	3.7
This work	0.120	1.44	1.81	0.0388	99.5	2.65	3.7

TABLE III. Water and cyanide models used in this study. The combination of them are called models 0 through 6. V_{bond} represents bonded interactions and V_{es} electrostatic interactions. q is electric charges, μ dipole moments, and Θ quadrupole moments. $r_{\text{min}} = r_{\text{UFF}}$ is used for CN^- in the case of M5, whereas $r_{\text{min}} = 1.075 r_{\text{UFF}}$ is used for all other models. "SHAKE" refers to simulations in which SHAKE is applied to all water molecules, as is typically done in biomolecular simulations. All models were run for 20 ns.

Model	SHAKE	$V_{\text{bond}}^{\text{water}}$	$V_{\text{es}}^{\text{water}}$	$V_{\text{bond}}^{\text{CN}^-}$	$V_{\text{es}}^{\text{CN}^-}$
M0	No	KKY	q_{TIP3P}	Morse	q, μ, Θ
M1	No	KKY	q, μ, Θ	Morse	q, μ, Θ
M2	No	TIP3P	q_{TIP3P}	Morse	$q_{3-\text{point}}$
M3	No	TIP3P	q_{TIP3P}	Morse	q, μ, Θ
M4	Yes	TIP3P	q_{TIP3P}	Morse	q, μ, Θ
M5	Yes	TIP3P	q_{TIP3P}	Morse	q, μ, Θ
M6	Yes	TIP3P	q_{TIP3P}	Harmonic	q_{CHELPG}

vibrational transition is

$$\omega = \frac{E_1 - E_0}{\hbar} = \omega_0 - \frac{\hbar\omega_0^2}{2D_e}, \tag{5}$$

where $\omega_0 = 2\pi\nu_0$.

B. Cumulant approximation

From the frequency trajectory $\omega(t)$, the frequency fluctuation $\delta\omega(t) = \omega(t) - \langle\omega(t)\rangle$ is obtained, where $\langle\omega(t)\rangle$ is the ensemble average, and the FFCF $\langle\delta\omega(0)\delta\omega(t)\rangle$ is computed. The FFCF can be used to determine the line shape function within the cumulant approximation[60]

$$g(t) = \int_0^t d\tau' \int_0^{\tau'} d\tau'' \langle\delta\omega(\tau'')\delta\omega(0)\rangle, \tag{6}$$

from which the linear response function is obtained as[60]

$$R_{\text{linear}} \propto |\vec{\mu}_{01}|^2 \langle\vec{u}(0)\cdot\vec{u}(t)\rangle e^{-i\omega_{01}t} e^{-g(t)}, \tag{7}$$

where $\vec{\mu}_{01}$ is the transition dipole moment. Here, the rotational part $\langle\vec{u}(0)\cdot\vec{u}(t)\rangle$, where $\vec{u}$ is the unit vector along the C–N bond, is explicitly included because for CN^- this contribution has been found to be essential.[26] Under circumstances when the rotational part does not contribute significantly to the line shape, $\langle\vec{u}(0)\cdot\vec{u}(t)\rangle = 1$ is usually used. This point will be discussed further below. From the line shape functions, one also obtains the rephasing and non-rephasing third-order response functions,[60]

$$\begin{aligned} R_{1,2,3} &\propto 2\mu_{01}^4 (e^{-i\omega_{01}(t_3-t_1)} - e^{-i((\omega_{01}-\Delta)t_3-\omega_{01}t_1)}) \\ &\quad \cdot e^{-g(t_1)+g(t_2)-g(t_3)-g(t_1+t_2)-g(t_2+t_3)+g(t_1+t_2+t_3)}, \\ R_{4,5,6} &\propto 2\mu_{01}^4 (e^{-i\omega_{01}(t_3+t_1)} - e^{-i((\omega_{01}-\Delta)t_3+\omega_{01}t_1)}) \\ &\quad \cdot e^{-g(t_1)-g(t_2)-g(t_3)+g(t_1+t_2)+g(t_2+t_3)-g(t_1+t_2+t_3)}, \end{aligned} \tag{8}$$

where t_1, t_2, and t_3 are delay times and $\Delta \equiv \omega_{01} - \omega_{12}$ is the anharmonic shift. Orientational effects are neglected in the third-order response functions given above. In the present work, $\Delta = 21.4\ \text{cm}^{-1}$ computed from the Morse potential parameters was used for $^{13}C^{15}N^-$, which agrees with the experimental value, $\Delta = 22\ \text{cm}^{-1}$, obtained for $^{13}C^{15}N^-$.[28]

To compute the line shape function $g(t)$, the FFCF can be integrated numerically. Alternatively, the FFCF can be fitted to a parametrized form and $g(t)$ can be found by analytic integration. Two different functional forms have been fitted to the FFCF

$$\langle\delta\omega(0)\delta\omega(t)\rangle = a_1 \cos(\gamma t) e^{-t/\tau_1} + a_2 e^{-t/\tau_2} + a_3 e^{-t/\tau_3} \tag{9}$$

and

$$\langle\delta\omega(0)\delta\omega(t)\rangle = a_1 \cos(\gamma t) e^{-t/\tau_1} + a_2 e^{-t/\tau_2}, \tag{10}$$

where a_1, a_2, a_3, τ_1, τ_2, τ_3, and γ are parameters.[60,61]

If the functional form of the FFCF given in Eq. (9) or (10) is used in the line shape function (Eq. (6)), the integration can be carried out in closed form.[60] However, the functional form of Eqs. (9) and (10) is unknown and a fit to it is highly nonlinear.

C. Non-cumulant treatment

If the cumulant approximation is avoided, the linear and 2D IR spectra can be calculated from the instantaneous frequencies and dipole moments according to Ref. 62

$$R_{\text{linear}} \propto \langle\mu_{01}(0)\mu_{01}(t) e^{-i\int_0^t \omega_{01}(\tau)d\tau}\rangle, \tag{11}$$

$$\begin{aligned} R_{1,2} &\propto \langle\mu_{01}(0)\mu_{01}(t_1)\mu_{01}(t_1+t_2)\mu_{01}(t_1+t_2+t_3) e^{i\int_0^{t_1}\omega_{01}(\tau)d\tau} e^{-i\int_{t_1+t_2}^{t_1+t_2+t_3}\omega_{01}(\tau)d\tau}\rangle, \\ R_{3} &\propto \langle\mu_{01}(0)\mu_{01}(t_1)\mu_{12}(t_1+t_2)\mu_{12}(t_1+t_2+t_3) e^{i\int_0^{t_1}\omega_{01}(\tau)d\tau} e^{-i\int_{t_1+t_2}^{t_1+t_2+t_3}\omega_{12}(\tau)d\tau}\rangle, \\ R_{4,5} &\propto \langle\mu_{01}(0)\mu_{01}(t_1)\mu_{01}(t_1+t_2)\mu_{01}(t_1+t_2+t_3) e^{-i\int_0^{t_1}\omega_{01}(\tau)d\tau} e^{-i\int_{t_1+t_2}^{t_1+t_2+t_3}\omega_{01}(\tau)d\tau}\rangle, \\ R_{6} &\propto \langle\mu_{01}(0)\mu_{01}(t_1)\mu_{12}(t_1+t_2)\mu_{12}(t_1+t_2+t_3) e^{-i\int_0^{t_1}\omega_{01}(\tau)d\tau} e^{-i\int_{t_1+t_2}^{t_1+t_2+t_3}\omega_{12}(\tau)d\tau}\rangle, \end{aligned} \tag{12}$$

where the angular brackets denote an average over configurations in the MD simulation. The transition dipole is treated as independent of frequency (the Condon approximation); this is justified by extensive quantum calculations that show no correlation between the transition dipole and frequency. In addition, the harmonic relation $\mu_{12} = \sqrt{2}\mu_{01}$ is used. Polarization effects are treated via spherical averaging.[63] An additional difference between Eqs. (11), (12) and Eqs. (7), (8)

is that the latter assume that the orientational and frequency correlation functions are separable whereas the former do not assume this.

Once the response functions $R_{1,\ldots,6}$ are known, the associated frequency-domain spectra are calculated via a double Fourier transform over t_1 and t_3. The 2D IR spectra in the frequency domain have been determined by Fourier transformation of the response function[60]

$$S_{\mathrm{r/nr}}(\omega_1, t_2, \omega_3) = \int_0^\infty \int_0^\infty R_{\mathrm{r/nr}}(t_1, t_2, t_3) e^{i\omega_1 t_1} e^{i\omega_3 t_3}\, dt_1\, dt_3 \tag{13}$$

After inverting the sign of ω_1 of the rephasing part, the real part of the sum of both rephasing (r) and non-rephasing (nr) spectra was taken to obtain the purely absorptive 2D IR spectra,

$$S_{\mathrm{abs}}(\omega_1, t_2, \omega_3) = \Re\left(S_{\mathrm{r}}(-\omega_1, t_2, \omega_3) + S_{\mathrm{nr}}(\omega_1, t_2, \omega_3)\right). \tag{14}$$

Using this method, spectra were obtained for waiting times t_2 ranging from 0 to 10 ps.

The tilt angle (or nodal slope) is an important experimental quantity which reports on the FFCF and hence provides a direct link to the MD simulations.[64] Within several approximations and for sufficiently long t_2, detailed analysis has shown the tilt angle to be related linearly to the FFCF,[65] while the tilt angle strongly underestimates the fast inertial component of the FFCF on timescales $\lesssim$ 100 fs. Here, the tilt angle of the nodal line between the 0–1 and the 1–2 peak was calculated from the 2D spectra. For each grid point along the ω_1 axis of the 2D spectrum, the position in the ω_3 axis that gives zero intensity (which corresponds to the point between the negative and positive peaks) is determined by linear regression of 4 points around the zero-intensity point. Next, a line connecting the zero-intensity points was determined by another regression, and the tilt angle was computed from the slope of the line.[28]

III. RESULTS

The main purpose of the present work is to establish a relationship between the force fields and their ability to capture the spectroscopy and dynamics of the solute. In particular, it will be of interest to determine whether the previously found improvements to the vibrational relaxation dynamics by (a) employing multipolar interactions and (b) somewhat modifying the van der Waals ranges also help to discriminate between more or less meaningful models for linear and 2D IR spectra. In order to limit the number of models to be pursued, we restrict the discussion to those that are found particularly realistic and interesting early on.

A. Linear spectra

From $g(t)$ computed by Eq. (6), the linear spectrum can be evaluated by Fourier transforming the expression $\langle \vec{u}(0) \cdot \vec{u}(t) \rangle e^{-g(t)}$ (see Eq. (7)). Corresponding line shapes from numerically computed $g(t)$ with center bands (ω_{01} in Eq. (7)) shifted to zero are shown in Figure 3. The full

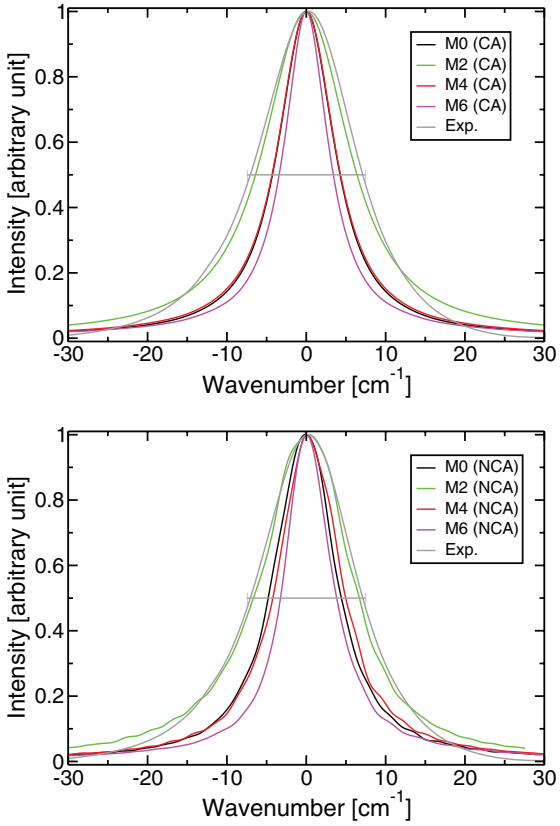

FIG. 3. 1D IR spectra for various models computed with cumulant approximation (label CA, upper panel) or without cumulant approximation (label NCA, lower panel). Rotational contribution of CN^- has been incorporated in the spectra for CA and NCA. M0 is shown in black, M2 in green, M4 in red, and M6 in magenta. FWHMs (in cm^{-1}) are 8.5 (M0), 9.0 (M1), 12.8 (M2), 8.6 (M4), 7.4 (M5), and 6.8 (M6) for CA and 9.2 (M0), 9.4 (M1), 13.3 (M2), 9.2 (M4), 7.4 (M5), and 7.1 (M6) for NCA. The experimental FWHM[27] is shown as a gray bar at height 0.5 and the gray solid line represents the experimental spectrum with water background removed.

widths at half maximum (FWHM) range from 6.8 to 12.8 cm^{-1} for the various models, when 1D spectra are generated by using the cumulant approximation and orientational effects are included. The FWHMs computed without using the cumulant approximation (Eq. (11)) range from 7.1 to 13.3 cm^{-1}. Experimentally, the widths of the IR, isotropic, and anisotropic Raman spectra of $^{12}C^{14}N^-$ in H_2O are 18, 8, and 19 cm^{-1}, respectively.[26] The IR line width reduces from 18 to 14.9 cm^{-1} for $^{13}C^{15}N^-$ in D_2O,[27] which was the isotope used in the present work for direct comparison with the experimental 2D IR spectra.[28] Other measurements of the Raman spectra of $^{12}C^{14}N^-$ yielded a FWHM of 7.5–11.6 cm^{-1}, depending on the concentration,[66] while previous simulations with $^{12}C^{14}N^-$ obtained a FWHM of 9 cm^{-1} for the isotropic Raman line shape. However, it should be noted that the width and peak height of the spectrum were controlled and that the spectral features could have been affected by filtering techniques.[29]

The most realistic 1D line shape from analysis without invoking the cumulant approximation[62,67] is found for model 2 (M2), which yields a FWHM of 13 cm^{-1}, in quite good agreement with the experimental value of 14.9 cm^{-1}.[27] All other models give lines that are narrower. For this

reason, the 2D spectra are discussed in more detail for model M2, together with M0 and M4. M0 is of interest as it was found to reliably capture the vibrational relaxation of CN^-, while M4 is the situation typically encountered in simulations where the water model is not flexible. The experimental spectrum, taken from the work of Hamm *et al.*,[27] is also displayed after subtraction of the D_2O background. It should be noted that background subtraction can be problematic, which makes straight inversion of the line shape function to yield the correlation function typically unreliable.[68] All simulations and analyses were also repeated for the other models and their results are reported in the text without detailed discussion. It is of interest to mention that with a conventional 2-point charge model (M6), i.e., a "conventional force field" for CN^-, the width of the linear spectrum is 6.8 cm^{-1} from using the cumulant approximation, which slightly increases to 7.1 cm^{-1} when avoiding this approximation.

The present analysis also allows us to verify that including the rotational part in Eq. (7) is indeed essential for the spectroscopy of CN^-. Typically (e.g., for pure water), the FWHM is dominated by the vibrational contribution, and the rotational part $\langle \vec{u}(0) \cdot \vec{u}(t) \rangle$ can be replaced by a constant μ_{01}^2 which yields $R_{\text{linear}} \propto \mu_{01}^2 e^{-i\omega_{01}t} e^{-g(t)}$. The FWHMs from such an analysis are 4.7 (M0), 3.7 (M1), 8.1 (M2), 4.3 (M4), 5.9 (M5), and 2.4 (M6). This is approximately a factor of 2 smaller than with the full analysis. Hence, the present simulations confirm that the rotational contribution is essential and also provides a correct quantitative description of this effect.

Alternatively, the analysis without the cumulant approximation can be carried out by evaluating $R_{\text{linear}} \propto \langle e^{-i\int_0^t \omega_{01}(\tau)d\tau} \rangle$ in Eq. (11). The FWHMs obtained from this are 4.2 (M0), 3.4 (M1), 7.7 (M2), 3.9 (M4), 5.1 (M5), and 2.5 (M6). Hence, we find again that the rotational contribution is essential and approximately doubles the linewidths.

Finally, the frequencies of $^{13}C^{15}N^-$ in the gas phase and in D_2O have been obtained from the 1D IR spectra computed from the Fourier transform of the dipole moment autocorrelation function. For the trajectories generated with M0, the gas-phase absorption peak occurs at 1885 cm^{-1} (FWHM of 0.65 cm^{-1}), whereas it is centered around 1921 cm^{-1} with a FWHM of 9.7 cm^{-1} in D_2O. This corresponds to a blue shift of 36 cm^{-1} for the spectrum in solution relative to that in the gas phase. Experimentally, the gas phase stretching frequency of $^{12}C^{14}N^-$ has been estimated to be at 2035 ± 40 cm^{-1} from photoelectron spectroscopy.[50] Accounting for the isotopic substitution, this corresponds to 1960 cm^{-1} for $^{13}C^{15}N^-$ and leads to a blue shift of ≈44 cm^{-1} for solvated $^{13}C^{15}N^-$ which was observed at 2004 cm^{-1}.[27] Given the considerable error bar in the gas phase value, the present simulations correctly reproduce the observed blue shift. For models M2 and M4, the gas-phase peak remains the same whereas that in solution is centered around 1944 and 1919, respectively. Hence, the multipolar models M0 and M4 give a blue shift of 35 cm^{-1} (Exp: ≈44 cm^{-1}) in somewhat better agreement with experiment than the 3-point charge model M2 for which the blue shift is 59 cm^{-1}. However, both values are still within the experimental error bars.

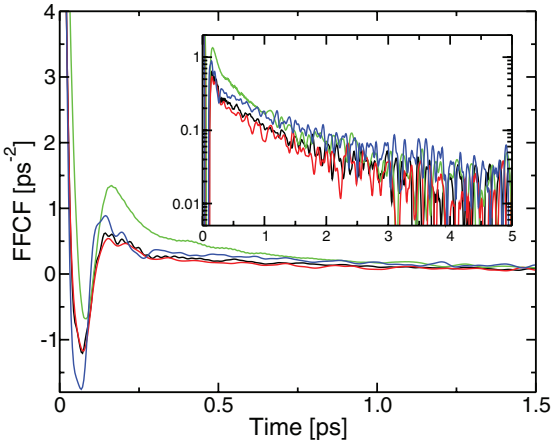

FIG. 4. The FFCFs from 0 to 1.5 ps obtained from the simulations of $^{13}C^{15}N^-$ in D_2O with M0 (black), M2 (green), M4 (red), and M5 (blue). All frequencies were computed with water molecules within 5 Å from CN^-. The inset shows FFCFs in the range of 0–5 ps on a logarithmic scale.

B. 2D spectra and tilt angles

In the following, FFCFs are discussed and the 2D spectra and the tilt angles determined from them are compared for models M0, M2, and M4 and with experiment. The FFCFs are reported in Figure 4. Three time scales can be distinguished in the FFCFs and are discussed further below.

As noted before, it is possible to fit the FFCF to empirical expressions (Eqs. (9) and (10)) from which the line shape function and the 2D IR spectrum can then be obtained analytically.[60] A comparison of the raw data with fits including two or three decay times is reported in Figure 5. The corresponding fitting parameters are summarized in Table IV. For models M0 and M4, the two short time scales were invariably sub-picosecond, with $\tau_1 \approx 0.04$ and τ_2 ranging from 0.8 to 1.0 ps. The third time scale τ_3 ranges from 9 to 21 ps. For M2, time constant τ_1 is similar to those from models M0 and M4, but somewhat shorter for τ_2 and very different for τ_3. For fits with more than three decay times, no new time scales seem to appear. As discussed further below, the value of τ_3 may be related to the timescale of the water dynamics around the ion.[26]

TABLE IV. Parameters obtained from fitting the FFCF. Equation (10) was fitted to FFCF data in the range of 0–20 ps for Fit 1 and Eq. (9) was used for Fit 2. For the calculation of CN^- frequencies for FFCFs, water molecules within 5 Å from CN^- have been included.

	M0		M2		M4	
	Fit 1	Fit 2	Fit 1	Fit 2	Fit 1	Fit 2
a_1	10.20	10.18	9.956	9.549	10.05	10.03
a_2	0.363	0.362	1.503	1.532	0.316	0.319
a_3	…	0.014	…	0.287	…	0.015
τ_1	0.039	0.039	0.054	0.056	0.039	0.039
τ_2	0.989	0.866	0.421	0.239	0.960	0.798
τ_3	…	9.151	…	1.489	…	20.99
γ	40.78	40.82	32.91	33.56	39.69	39.75
χ^2	3.941	3.840	4.371	1.984	4.312	3.993

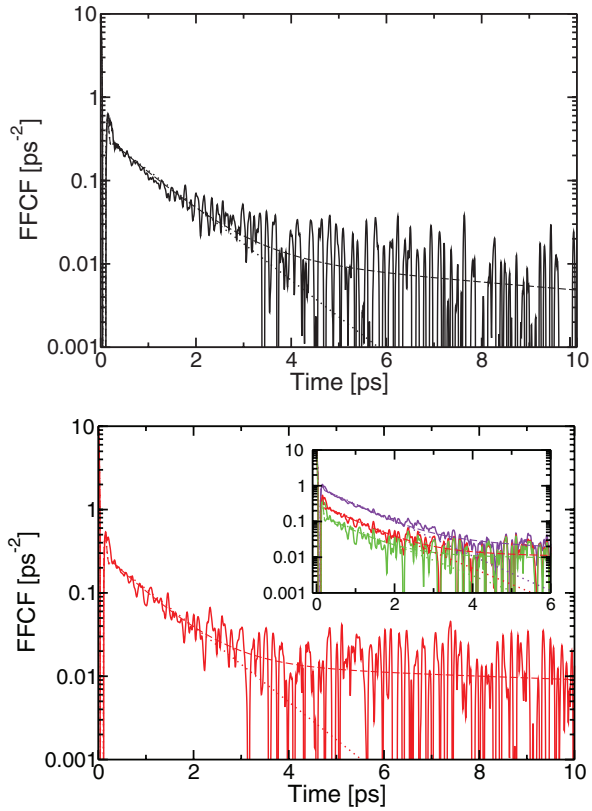

FIG. 5. Fitting of Eq. (9) or (10) to the FFCFs obtained from the trajectories of $^{13}C^{15}N^-$ in D_2O with models 0 (upper panel) and 4 (lower panel). Logarithmic scale is used for the vertical axis. Raw FFCFs are shown in solid lines, fitting with Eq. (9) in dashed lines, and fitting with Eq. (10) in dotted lines. In the inset of the lower panel, FFCFs obtained from the frequency calculation of CN^- with water molecules within 3 Å (violet), 5 Å (red), and ∞ (green) from CN^- are compared.

Experimentally, two time scales for the decay of the FFCF were reported: $\tau_1 = 0.2$ ps, $\tau_2 = 2.9$ ps.[28] These results compare with reported correlation times $\tau_1 = 0.043$ ps and $\tau_2 = 0.3$ ps (estimated) from previous simulations.[29] Experimentally, decay times on the several 10 fs time scale (i.e., the shortest τ from the simulations) cannot be determined with confidence. Hence, decay times of 1–10 ps, corresponding to the computed τ_2 and τ_3, are within the measured decay time. However, we note that the fitted decay times to the experimental data do not faithfully reproduce the experimentally measured tilt angle $\alpha(t_2)$ at longer times ($t_2 \geq 5$ ps).[28] The present computations agree with previous simulations on the existence of two sub-picosecond time scales and strongly suggest that a considerably longer relaxation time, on the 10 ps time scale, is present.

2D IR spectra of $^{13}C^{15}N^-$ in D_2O have been determined from the simulations performed with the various interaction models. Analyses with and without invoking the cumulant approximation were carried out. As a test, 2D IR spectra within the cumulant approximation were also determined by using the line shape function obtained from the analytic integration of the fitted FFCF. The force fields used in M0 simulations (see Tables I–III) can be considered physically motivated as they quantitatively describe the vibrational relaxation of CN^- in H_2O and D_2O.[30] In addition to multipolar electrostatics, it was also necessary to scale the LJ range parameter of the C and N atoms by 7.5% ($r_{min} = 1.075 r_{UFF}$), as is further discussed below. Without such scaling, the vibrational relaxation times would be too short, whereas their ratio in the two solvents are correctly described. The 2D IR spectra for M0 with and without the cumulant approximation at waiting times $t_2 =$ 100 fs, 1 ps, and 10 ps are shown in Figure 6. The 2D spectra displayed in Figure 6 are generally in good agreement with the experimental results,[28] which may be related to the fact that MD simulations with M0 quite realistically reproduce the 1D IR line shape. The 2D spectra from M4 look similar to those from M0, and thus they are not shown.

As mentioned above, the tilt angle $\alpha(t_2)$ can be used to directly relate the experimental spectra with the MD simulations. From the data in Figure 6, α as a function of evolution time t_2 has been determined (see Sec. II). The left panel of Figure 7 reports tilt angles computed from the line shape functions obtained by the numerical integration of the FFCFs for various models. In the inset of the left panel, we compare the difference between the tilt angles from the numerical line shape function mentioned above (solid circle) and from the analytical line shape function obtained from fitting of Eq. (9) to FFCFs (open circle) for M0. As can be seen, the difference in the tilt angles computed from the numerical and analytical line shape functions is small. In the right panel, the tilt angles computed without using the cumulant approximation are shown. The inset of the right panel compares the difference between the tilt angles computed with (solid circle) and without (open circle) using the cumulant approximation for M0. As can be seen, the general trend is comparable, but the tilt angles without using the cumulant approximation give better agreement with experiment, possibly due to the neglect of the effect of rotation in the case of the cumulant approximation. $\alpha(t_2)$ decays virtually to zero on the 10 ps time scale for several computed spectra – in particular when using the cumulant approximation – whereas the experimentally determined $\alpha(t_2)$ has still a finite value at $t_2 = 10$ ps. This is better captured from analyzing the trajectories without using the cumulant approximation. Simulations with a conventional point-charge model (M6) do not capture the tilt angle particularly well and $\alpha(t_2)$ decays much too rapidly as a function of t_2. On the contrary, the MTP or 3-point charge models for CN^- give a very realistic description for $\alpha(t_2)$. The oscillations in $\alpha(t_2)$, specifically for small tilt angles, can be related to the way how the tilt angle was determined from the 2D spectra (see Sec. II). This was verified by repeating the analysis with a varying number of points ranging from 3 to 7 from which the center line slope was determined. Typically, the tilt angle varied within 2° for the different analyses.

In our previous work on the vibrational energy relaxation of cyanide in water,[30] the flexibility of water played an important role in intermolecular energy transfer, as the bending mode of water accepted vibrational energy. The effect of water flexibility can be illustrated by comparing results from models M3 (without SHAKE) and M4 (with SHAKE). It is found that the FFCF of M3 differs slightly from that of M4, causing a small difference in the decay of $\alpha(t_2)$. With M4, $\alpha(t_2)$ decays slightly more slowly than with M3. Thus, SHAKE indeed has an effect on the results, albeit a small one.

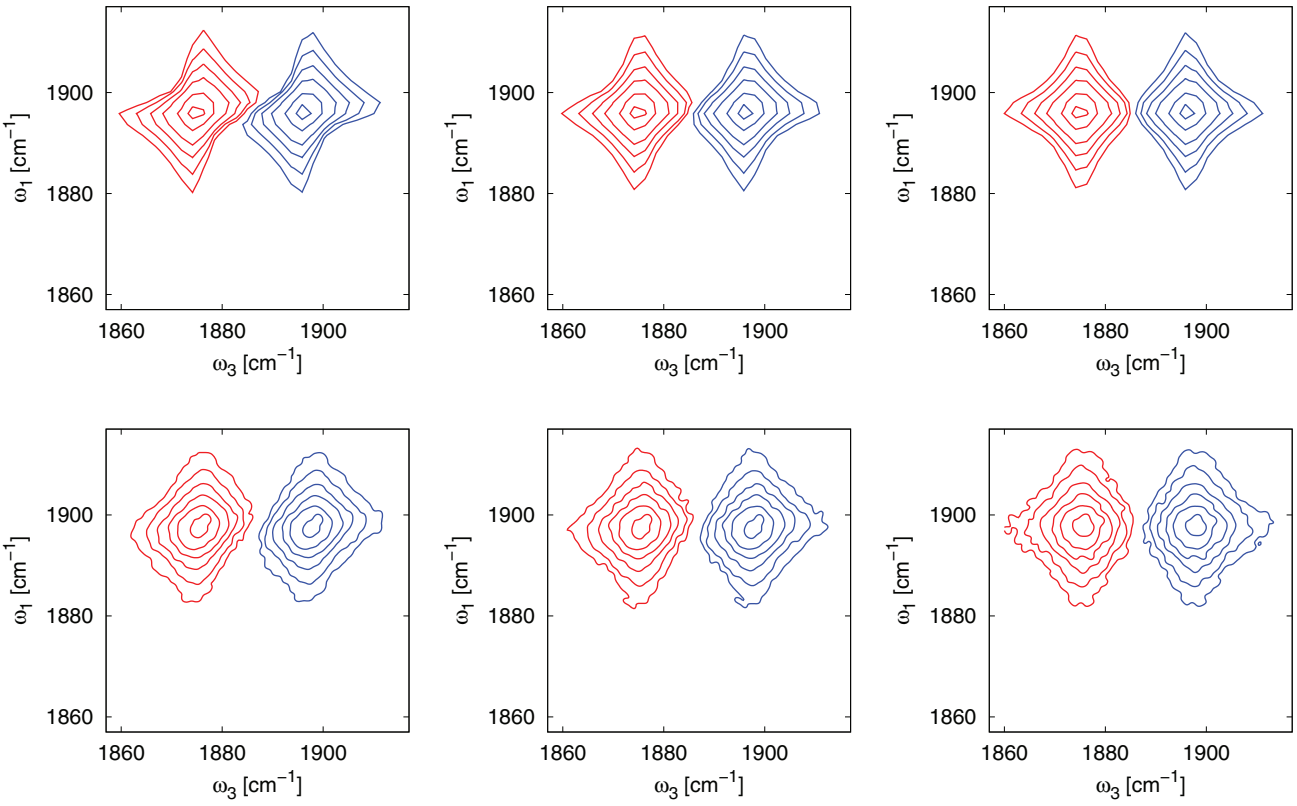

FIG. 6. The 2D IR spectra of $^{13}C^{15}N^-$ in D_2O using model M0 computed using the cumulant approximation with numerically integrated $g(t)$ (1st row) and avoiding the cumulant approximation (2nd row). Waiting times are 100 fs (1st column), 1 ps (2nd column), and 10 ps (3rd column).

In addition to simulations with rigid water molecules, we carried out simulations with M4 for a rigid CN^-, where the C–N and O–H bond lengths were constrained to their equilibrium values using SHAKE. The FFCF thus obtained very closely matches that from simulations with a flexible CN^-.

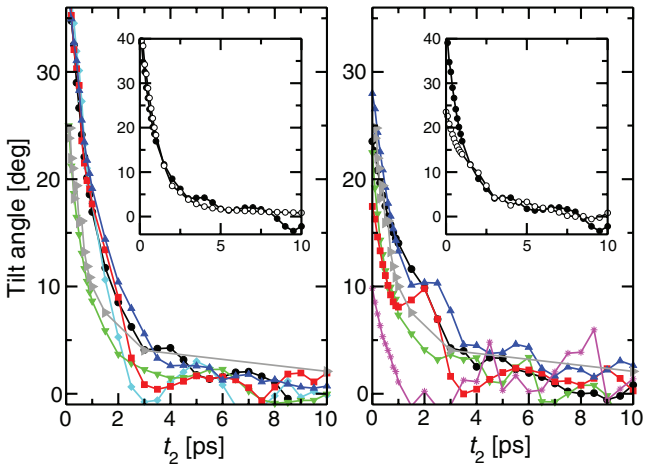

FIG. 7. Comparison of tilt angles as a function of mixing time t_2. Left panel shows $\alpha(t_2)$ determined using the cumulant approximation with the line shape functions $g(t)$ obtained from FFCFs by numerical integration (solid lines). The inset compares the tilt angles from the numerical (solid circle) and the analytical line shape functions obtained from fitting of Eq. (9) to the FFCF (open circle) for M0. Black curve is from M0, cyan from M1, green from M2, red from M4, and blue from M5. Right panel shows $\alpha(t_2)$ determined by avoiding the cumulant approximation and the inset compares the tilt angles computed with (solid circle) and without (open circle) using the cumulant approximation for M0. The color scheme for M0, M2, M4, and M5 is the same as the left panel and M6 is shown in magenta. For comparison, tilt angles from experiment[28] are shown in gray in both panels.

The influence of modifying the van der Waals ranges of the C and N atoms on the 2D IR spectra and on $\alpha(t_2)$ was also assessed. In previous work,[30] it was found that the relative vibrational relaxation times for CN^- in H_2O versus D_2O could be correctly captured with accurate multipolar electrostatics. However, to obtain quantitative agreement with experiment, the van der Waals ranges needed to be slightly increased by ≈7.5% in order to reproduce the experimentally determined relaxation times. While $r_{min} = 1.075 r_{UFF}$ was used in most of the simulations in the present work, one trajectory was run with $r_{min} = r_{UFF}$ – i.e., model M5 – for comparison (see Sec. II). The FFCF obtained from simulations with M5 (blue line in Figure 4) decays more slowly compared to that with M4. This also affects the line shapes of the 2D IR spectra and the behavior of $\alpha(t_2)$. In particular, it is found that slight changes to the van der Waals ranges have more prominent effects than changes in the simulation conditions such as SHAKEing the water solvent or the CN^- bond length. Comparison with the linear and 2D IR experiments suggests that a multipolar model, such as M0 or M4, with $r_{min} = 1.075 r_{UFF}$ is preferable over M5 with $r_{min} = r_{UFF}$. However, the effects are less prominent than for vibrational energy relaxation.

Finally, we also comment on the computation of the stretching frequency ω of the oscillator for a given solvent conformation. In the present work, ω has been determined from an instantaneous potential energy curve for which the surrounding water molecules were frozen and only the CN^- distance was allowed to vary along the bond. For distances

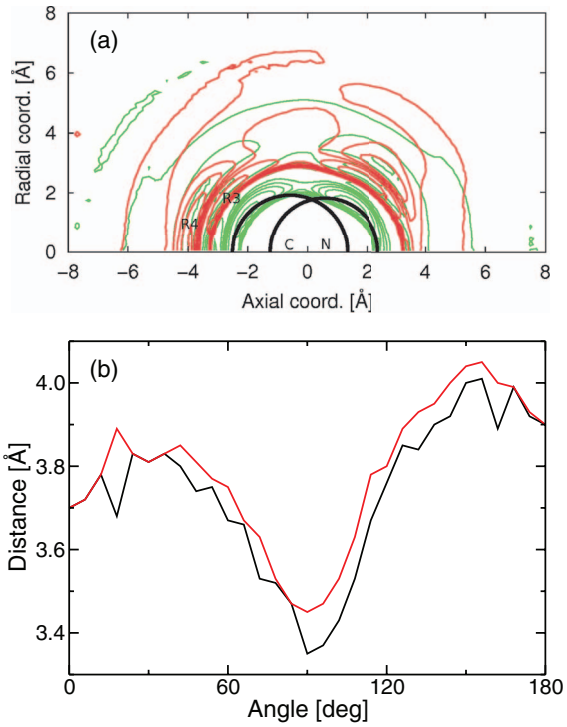

FIG. 8. (a) The distribution of water molecules around CN^- computed from the simulations with M0. The geometric center of CN^- is at the origin, and the probability of finding water oxygen atoms at certain axial and radial distances from CN^- is displayed in red contour. The maximum around $R \approx 3$ Å is labeled as "R3" and the maximum around $R \approx 4$ Å as "R4." The probability of hydrogen atoms is displayed in green. The van der Waals radii of carbon and nitrogen atoms are shown in black semicircles. (b) The distance of the first radial *minimum* from the origin as a function of the angle with respect to the axial coordinate, computed from the distribution of water molecules around CN^-. The result from M0 is shown in black and that from M4 in red.

shorter than the instantaneous CN^- bond length, there should be no artifacts. However, when the CN^- bond is stretched, the van der Waals spheres of the C and N atoms start to overlap with those of the surrounding water molecules and may overestimate the repulsion.

C. Solvent dynamics

Once a particular simulation environment (force field, dynamics, analysis) has been validated in view of experimental data, the essential benefit of MD simulations is the availability of the conformations that lead to the observed properties. These conformations are not readily available from experiment and allow the investigation of additional atomistic aspects (and details) of the system. In the following, we also attempt to correlate the frequency response of CN^- with the structural dynamics in the surrounding solvent shell. From the configurations sampled, the solvent density around the ion can be determined (see Figure 8). It is found that the distribution functions differ only slightly between M0 and M4 (Figure 8(b)). A first solvation ring, consisting of two pronounced D_2O-density maxima, is found at distances 2.8–3.6 Å from the center of the CN^- ion. The maxima are slightly asymmetric, which reflects the non-symmetric charge distribution around the ion. A second, more diffuse solvent ring appears at distances around 4–6 Å away from the center of the ion.

These geometrical parameters are further used to analyze the solvent exchange dynamics near the ion. To this end, residence times of D_2O molecules surrounding the ion were determined. The analysis for M0 or M4 finds an average of 9 D_2O molecules in the inner shell ($R \leq 4$ Å). To compute the residence time, the number of consecutive steps where the O atom of D_2O is within 4 Å from the center of the cyanide ion has been counted for each water molecule from the trajectory. In many cases, the water oxygen atom escapes slightly from the inner shell ($R \leq 4$ Å) and then re-enters the shell. Therefore, once an oxygen atom enters within 4 Å of CN^-, it is considered to be in the solvation shell as long as the oxygen atom is within R_{cut} from CN^-, where R_{cut} is somewhat larger than the shell radius. R_{cut} values of 5.5, 6.0, and 6.5 Å have been tested. Depending on the cutoff distance R_{cut}, the residence times change somewhat. For $R_{cut} = 5.5$ Å, the residence times are 6.1 and 5.5 ps for M0 and M4, respectively. They change to 9.0 and 8.0 ps for $R_{cut} = 6.0$ Å and to 12.4 and 10.8 ps for $R_{cut} = 6.5$ Å. Inspection of Figure 8(a) suggests that an adequate value is $R_{cut} \approx 6$ Å for which residence times are typically 10 ps. This time scale is considered representative for outer-shell solvent exchange.

Similar analyses were carried out for distances of the water oxygen atom from the center of CN^- in the range of $R \leq 3.5$ Å, together with $R_{cut} = 4$ Å. This yielded residence times of about 2 ps and corresponds to inner-shell solvent exchange. Comparison with the decay times of the FFCF suggests that the long time decay ($\tau_3 \approx 9$ ps) could be associated with outer-shell water exchange whereas the shorter time scales ($\tau_2 \approx 1$ ps) could be potentially related to inner-shell solvent exchange. It is interesting to note that the interpretation of nuclear mangetic resonance (NMR) experiments found a water-residence time of at least 8 ps in the solvation sphere and the reported duration for the ion-water interaction is 1 ps.[26] From the above analysis, we associate the ≈10 ps time scale with water exchange between regions $R < 4$ Å and $R > 6$ Å.

Additional insight into the solvent dynamics can be obtained from considering solvent-shell occupation fluctuation correlation functions. They are constructed from counting the number $n(t)$ of D- and O-atoms, respectively, of the D_2O solvent surrounding the CN^- up to a maximal distance of 3 and 4 Å, respectively. From this, $C_n(t) = \langle \delta n(0) \delta n(t) \rangle / \langle [\delta n(0)]^2 \rangle$ is constructed, where $\delta n(t) = n(t) - \langle n \rangle$ and $\langle n \rangle$ is the average occupation number over the entire trajectory. The results from the simulations with M0 and M4 are reported in Figure 9. $C_n(t)$ decays on a sub-picosecond time scale. This is consistent with findings for azide, where such correlation functions were also determined.[69] It is also of interest to determine the decay of the correlation function constructed from $\delta H(t)$, which is shown in the inset of Figure 9. The characteristic function $H(t)$ for a water molecule is defined as 1 if the distance R between the water oxygen atom and the center of CN^- is less than 4 Å and $H(t) = 0$ if $R > 4$ Å. This is similar to the characteristic function used in the context of hydrogen-bonding by Lawrence and Skinner.[70] The correlation function $C_H(t) = \langle \delta H(0) \delta H(t) \rangle / \langle [\delta H(0)]^2 \rangle$ is obtained by considering

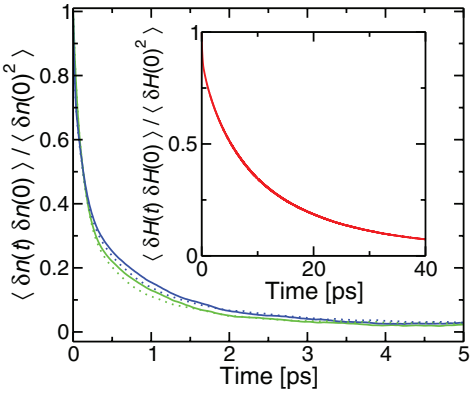

FIG. 9. The occupation fluctuation correlation function $C_n(t)$ of $\delta n(t)$ as a function of time. The solid lines are from M0 and the dotted lines from M4 for oxygen (green) and deuterium (blue) atoms with cutoff radius of 4 Å. The inset shows the occupation correlation function $C_H(t)$ of $\delta H(t)$ as a function of time for M4.

all water molecules for which $H(t) = 1$ at least once during the simulations, while those water molecules for which $H(t) = 0$ all the time during the entire simulations are not taken into account. $C_H(t)$ reports on the physical presence or absence of solvent molecules within a given range of the ion rather than the fluctuation and has characteristic time scales of several picoseconds. It thus corresponds to the physical diffusion time scale of solvent molecules in and out of particular solvent shells.

An additional point that can be discussed from the present simulations is the rotational contribution to the 1D line shape.[26] Several models for the solvent surrounding a solute have been put forward and discussed, ranging from "gas-like" (e.g., Gordon's M and J model[71]) to "solid-like" (Ivanov's jump model[72]). Gordon's model considers rotational reorientation as a sequence of collisions between solvent and solute, whereas in the jump model a reorientation is the consequence of an instantaneous repositioning between two definite positions. In the limit of negligible collision time for the Gordon model and for the jump angle to approach zero, both models correspond to the Debye model for which the correlation times of $G_1 = \langle \vec{u}(0) \cdot \vec{u}(t) \rangle$ and $G_2 = \frac{1}{2} \langle 3(\vec{u}(0) \cdot \vec{u}(t))^2 - 1 \rangle$ differ by a factor of 3. Such an analysis was carried out from the present trajectories. The rotational correlation times, defined as $\tau_{nR} = \int_0^\infty G_n(t)dt$, range from $\tau_{1R} = 1.71$ to 2.84 ps whereas $\tau_{2R} = 0.93$ to 1.19 ps for M0, M2, and M4. Thus, we find that the correlation times differ by a factor of ≈2 rather than 3 as is characteristic for the Debye model.

Conversely, we also followed the reorientation dynamics of the CN^- directly by considering the orientation of the C–N unit vector $\vec{u}(t)$. The relative angular change was followed as a function of simulation time by observing $\vec{u}(0) \cdot \vec{u}(t)$. A typical portion of such a dynamics is shown in Figure 10 as well and demonstrates that $\vec{u}(t)$ reorients on a time scale of several picoseconds in abrupt changes. The angular jumps can occur through different angles ranging from ≈50° to 100°. However, entire revolutions by 180° can also occur occasionally. The microscopic dynamics supports a picture in which discrete jumps at definite times are superimposed on rapid librational motions.

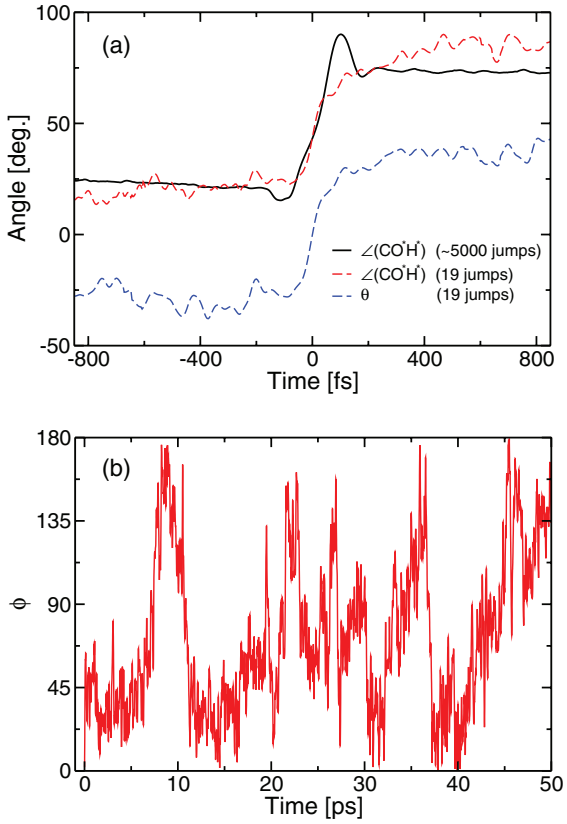

FIG. 10. (a) Analysis of the jump angle between cyanide and the neighboring water at the carbon-end of CN^-. θ is the angle between the rotating O*H* bond and the bisector plane of the CO*O′ angle, where O′ is the new H-bond acceptor.[73] (b) The change of direction of CN^- measured by $\vec{u}(0) \cdot \vec{u}(t)$ for 50 ps.

The experimental line shapes were analyzed in terms of the rotational dynamics based on several models, including those mentioned previously (*vide supra*).[26] The one favored by Lascombe and Perrot finds a ratio $\tau_{1R}/\tau_{2R} \approx 1$ based on a model which assumes angular jumps through 90° to 120° having a width $\sigma = 60°$ for the Gaussian distribution $e^{(\theta-\theta_0)^2/\sigma^2}$. The present simulations partly support such a model but clarify that the jump angles can even amount to 180° and that the typical rotation time is probably somewhat longer than 0.3 ps so that τ_{1R}/τ_{2R} is close to 2.[26]

The reorientational dynamics can also be investigated along the lines of recent work in which the water dynamics around monoatomic ions was considered.[73] Here, we restrict the discussion to the water dynamics around the carbon-end of cyanide. Two different analyses were carried out. One of them was identical to that presented recently for water dynamics around Cl^-.[73] It considers the angle θ between the rotating O*H* bond and the bisector plane of the CO*O′ angle, where O*H* is initially hydrogen bonded to the carbon atom of CN^- and O′ is the new acceptor to which H* binds. Alternatively, the C···O*–H* angle was considered, where O* and H* are the oxygen and hydrogen atoms of the water molecule H-bonded to the carbon-end of CN^-. It is important to note that due to the different selection criteria in the first analysis the number of events detected along the 20 ns simulation is rather low (≈ 20) whereas for the second analysis several

thousand events could be analyzed. In order to validate the use of the C$\cdots$O*–H* angle, the events found by considering θ were also analyzed with the C$\cdots$O*–H* angle. Whenever the angle considered changed abruptly, a segment of the trajectory around the change was stored, the time of the jump was defined as $t = 0$ and all the events were averaged. The results of this analysis are reported in Figure 10. The average C$\cdots$O*–H* jump angle is $\approx 60^\circ$. This is in qualitative agreement with the work on the reorientational dynamics of water around simple ion.[73]

IV. DISCUSSION AND CONCLUSIONS

Previous successful approaches to computing characteristics of three-pulse photon echo experiments were championed by Skinner and co-workers.[69,74] The approach is based on sampling the conformations with a parametrized force field and evaluating the FFCF from optimized quantum mechanics/molecular mechanics calculations. For the azide ion (N_3^-) in water, this optimized quantum mechanical/molecular mechanical (OQM/MM) approach proved to be superior to other strategies, including (extended) system-bath coupling, electrostatic electronic structure, or an empirical frequency correlation. The OQM/MM methodology applied to N_3^- in water required two parametrizations to be carried out – one for the force field to sample the structures, and one to improve the PM3 Hamiltonian to provide realistic frequencies. In the present work, we showed that from a carefully refined force field, based on physical interactions including Morse oscillators for all bonds and multipolar electrostatics for the probe molecule, it is possible to obtain a realistic description of the FWHM of the linear IR spectrum, correct characteristics of the FFCF, and tilt angles in quite good agreement with experiment.

It is well-known that the population relaxation time T_1 computed from classical molecular dynamics simulations differs from the quantum mechanical value in general; quantum correction factors must be introduced to compensate for the difference, although classical simulations can give accurate estimates of T_1 in special cases.[75–78] As opposed to T_1, the dephasing time can be evaluated more accurately by classical simulations, because changes in the vibrational frequency primarily depend on lower-frequency fluctuations, which can be captured by classical simulations. As the 2D IR line shape is sensitive to these lower-frequency fluctuations, classical simulations with sufficiently sophisticated electrostatics can be used to describe the 2D line shapes, even though the classical simulations may not be capable of reproducing T_1 very well.

This work investigates the computation of linear and 2D IR spectra for $^{13}C^{15}N^-$ in D_2O using different interaction models (M0 to M6). It is found that within a range of justifiable (and commonly used) force fields, the tilt angle α as a function of the waiting time can be realistically modelled. The conformational dynamics and the 1D and 2D spectra were computed from the same model, avoiding the use of frequency maps. Most importantly, a recently developed multipolar model for water and cyanide combined with anharmonic stretching and bending potentials[30] and slightly modified van der Waals ranges for the CN^- yields very favorable agreement with experiments,[28] without further adjustment of any parameter. It is concluded that such models provide a robust and realistic parametrization for dynamical problems including vibrational relaxation and 2D IR spectroscopy. In view of its good performance for the 1D line shape and describing the tilt angle, the vibrational relaxation time was also determined for M2. Contrary to experiment, the relaxation time in H_2O is longer than in D_2O. Hence, M0, which correctly describes vibrational energy relaxation and the spectroscopic properties investigated in the present work, is the preferred one.

The general procedure outlined in the present work can be applied to other diatomic probes to study dynamical processes on fast time scales. The time scales which appear in the FFCFs can be attributed to structural dynamics in the first and second solvation shells by considering solvent-shell occupation and solvent-shell fluctuation correlation functions. Such insight can probably only be gained from atomistic simulations once they have been validated with experiment as has been done in the present work. In the case of CN^- in D_2O, the time scales found for these processes are in reasonable agreement with NMR experiments.

It is noteworthy that, while the correlation times of $G_1 = \langle \vec{u}(0) \cdot \vec{u}(t) \rangle$ and $G_2 = \langle 3[\vec{u}(0) \cdot \vec{u}(t)]^2 - 1 \rangle / 2$ for the Debye model differ by a factor of 3, the ratio of the rotational correlation times computed in the present work is $\tau_{1R}/\tau_{2R} \approx 2$, which indicates that there can be instantaneous rotational jumps of the cyanide ion through finite angles.[26] This is supported by the analyses of our trajectories, which show that there are abrupt jumps of CN^- and that the vector of O*–H* originally H-bonded to CN^- rotates in less than 350 fs by $\sim 60^\circ$.

Force fields can be refined to a degree which allows them to quantitatively describe experimental observables ranging from vibrational energy relaxation to 2D IR spectroscopy. Because phase space can be sampled extensively with force fields, convergence of the results can be monitored. The present work highlights that parametrizations suitable for one type of observable are transferable to determining other observables, and that slight changes in the parametrization do have noticeable effects. The real potential of atomistic simulations becomes apparent when a computational model is validated in comparison with a range of experimental data, justifying the analysis of the underlying dynamics in view of properties which are not directly accessible to experiments. In this way, experiment and simulation provide a more complete description and understanding of complex dynamical processes.

ACKNOWLEDGMENTS

The authors gratefully acknowledge financial support from the Swiss National Science Foundation (NSF(CH)) through the NCCR-MUST (to M.M. and P.H.) and grant 200021-117810 (to M.M.). The research at the University of Wisconsin was supported in part by National Science Foundation (NSF) Grant No. CHE-0840494. The authors thank Professor J. L. Skinner for insightful discussions, and M.M. thanks the Chemistry Department of the University of Wisconsin for hospitality during the time in which part of this work has been carried out.

[1] Y. S. Kim and R. M. Hochstrasser, Proc. Natl. Acad. Sci. U.S.A. **102**, 11185 (2005).
[2] J. R. Zheng, K. Kwak, J. Asbury, X. Chen, I. R. Piletic, and M. D. Fayer, Science **309**, 1338 (2005).
[3] D. Laage, G. Stirnemann, F. Sterpone, and J. T. Hynes, Acc. Chem. Res. **45**, 53 (2012).
[4] G. Stirnemann, P. J. Rossky, J. T. Hynes, and D. Laage, Faraday Discuss. **146**, 263 (2010).
[5] D. Laage and J. T. Hynes, Science **311**, 832 (2006).
[6] J. B. Asbury, T. Steinel, K. Kwak, S. A. Corcelli, C. P. Lawrence, J. L. Skinner, and M. D. Fayer, J. Chem. Phys. **121**, 12431 (2004).
[7] J. B. Asbury, T. Steinel, C. Stromberg, S. A. Corcelli, C. P. Lawrence, J. L. Skinner, and M. D. Fayer, J. Phys. Chem. A **108**, 1107 (2004).
[8] S. A. Corcelli, C. P. Lawrence, J. B. Asbury, T. Steinel, M. D. Fayer, and J. L. Skinner, J. Chem. Phys. **121**, 8897 (2004).
[9] T. Steinel, J. B. Asbury, S. A. Corcelli, C. P. Lawrence, J. L. Skinner, and M. D. Fayer, Chem. Phys. Lett. **386**, 295 (2004).
[10] J. Stenger, D. Madsen, P. Hamm, E. T. J. Nibbering, and T. Elsaesser, Phys. Rev. Lett. **87**, 027401 (2001).
[11] J. Stenger, D. Madsen, P. Hamm, E. T. J. Nibbering, and T. Elsaesser, J. Phys. Chem. A **106**, 2341 (2002).
[12] C. J. Fecko, J. D. Eaves, J. J. Loparo, A. Tokmakoff, and P. L. Geissler, Science **301**, 1698 (2003).
[13] C. J. Fecko, J. J. Loparo, S. T. Roberts, and A. Tokmakoff, J. Chem. Phys. **122**, 054506 (2005).
[14] M. L. Cowan, B. D. Bruner, N. Huse, J. R. Dwyer, B. Chugh, E. T. J. Nibbering, T. Elsaesser, and R. J. D. Miller, Nature (London) **434**, 199 (2005).
[15] J. D. Eaves, J. J. Loparo, C. J. Fecko, S. T. Roberts, A. Tokmakoff, and P. L. Geissler, Proc. Natl. Acad. Sci. U.S.A. **102**, 13019 (2005).
[16] A. Tokmakoff, Science **317**, 54 (2007).
[17] T. Elsaesser, Acc. Chem. Res. **42**, 1220 (2009).
[18] S. T. Roberts, K. Ramasesha, and A. Tokmakoff, Acc. Chem. Res. **42**, 1239 (2009).
[19] A. Luzar and D. Chandler, Nature (London) **379**, 55 (1996).
[20] A. Luzar and D. Chandler, Phys. Rev. Lett. **76**, 928 (1996).
[21] P. L. Geissler, C. Dellago, D. Chandler, J. Hutter, and M. Parrinello, Science **291**, 2121 (2001).
[22] Y. S. Kim, L. Liu, P. H. Axelsen, and R. M. Hochstrasser, Proc. Natl. Acad. Sci. U.S.A. **105**, 7720 (2008).
[23] Y. S. Kim, L. Liu, P. H. Axelsen, and R. M. Hochstrasser, Proc. Natl. Acad. Sci. U.S.A. **106**, 17751 (2009).
[24] A. Remorino, I. V. Korendovych, Y. Wu, W. F. DeGrado, and R. M. Hochstrasser, Science **332**, 1206 (2011).
[25] J. Zheng, K. Kwak, J. Xie, and M. D. Fayer, Science **313**, 1951 (2006).
[26] J. Lascombe and M. Perrot, Faraday Discuss. Chem. Soc. **66**, 216 (1978).
[27] P. Hamm, M. Lim, and R. M. Hochstrasser, J. Chem. Phys. **107**, 10523 (1997).
[28] M. Koziński, S. Garrett-Roe, and P. Hamm, Chem. Phys. **341**, 5 (2007).
[29] R. Rey and J. T. Hynes, J. Chem. Phys. **108**, 142 (1998).
[30] M. W. Lee and M. Meuwly, J. Phys. Chem. A **115**, 5053 (2011).
[31] C.-H. Kuo and R. M. Hochstrasser, Chem. Phys. **341**, 21 (2007).
[32] H. Lee, G. Lee, J. Jeon, and M. Cho, J. Phys. Chem. A **116**, 347 (2012).
[33] J. Jeon and M. Cho, New J. Phys. **12**, 065001 (2010).
[34] M. Cho, Chem. Rev. **108**, 1331 (2008).
[35] J.-H. Choi, H. Lee, K.-K. Lee, S. Hahn, and M. Cho, J. Chem. Phys. **126**, 045102 (2007).
[36] M. Cho, Bull. Korean Chem. Soc. **27**, 1940 (2006).
[37] K. Kwac and M. Cho, J. Chem. Phys. **119**, 2256 (2003).
[38] M. Yang and J. L. Skinner, J. Chem. Phys. **135**, 154114 (2011).
[39] B. M. Auer and J. L. Skinner, J. Chem. Phys. **128**, 224511 (2008).
[40] R. Rey, K. B. Møller, and J. T. Hynes, J. Phys. Chem. A **106**, 11993 (2002).
[41] B. R. Brooks, R. E. Bruccoleri, B. D. Olafson, D. J. States, S. Swaminathan, and M. Karplus, J. Comput. Chem. **4**, 187 (1983).
[42] N. Plattner and M. Meuwly, Biophys. J. **94**, 2505 (2008).
[43] S. Nosé, J. Chem. Phys. **81**, 511 (1984).
[44] W. G. Hoover, Phys. Rev. A **31**, 1695 (1985).
[45] S. Midda and A. K. Das, Int. J. Quantum Chem. **98**, 447 (2004).
[46] A. K. Rappé, C. J. Casewit, K. S. Colwell, W. A. Goddard III, and W. M. Skiff, J. Am. Chem. Soc. **114**, 10024 (1992).
[47] C. M. Breneman and K. B. Wiberg, J. Comput. Chem. **11**, 361 (1990).
[48] A. J. Stone, J. Chem. Theory Comput. **1**, 1128 (2005).
[49] M. J. Frisch, G. W. Trucks, H. B. Schlegel, *et al.*, GAUSSIAN 03, Revision B.01, Gaussian, Inc., Pittsburgh, PA, 2003.
[50] S. E. Bradforth, E. H. Kim, D. W. Arnold, and D. M. Neumark, J. Chem. Phys. **98**, 800 (1993).
[51] C. Kramer, P. Gedeck, and M. Meuwly, J. Comput. Chem. **33**, 1673 (2012).
[52] J. E. Straub and M. Karplus, Chem. Phys. **158**, 221 (1991).
[53] D. R. Nutt and M. Meuwly, Biophys. J. **85**, 3612 (2003).
[54] D. R. Nutt and M. Meuwly, ChemPhysChem **5**, 1710 (2004).
[55] N. Kumagai, K. Kawamura, and T. Yokokawa, Mol. Simul. **12**, 177 (1994).
[56] W. L. Jorgensen, J. Chandrasekhar, J. D. Madura, R. W. Impey, and M. L. Klein, J. Chem. Phys. **79**, 926 (1983).
[57] J.-P. Ryckaert, G. Ciccotti, and H. J. C. Berendsen, J. Comput. Phys. **23**, 327 (1977).
[58] M. Yoneya, H. J. C. Berendsen, and K. Hirasawa, Mol. Simul. **13**, 395 (1994).
[59] N. Plattner, M. W. Lee, and M. Meuwly, Faraday Discuss. **147**, 217 (2010).
[60] P. Hamm and M. Zanni, *Concepts and Methods of 2D Infrared Spectroscopy* (Cambridge University Press, Cambridge, 2011).
[61] K. B. Møller, R. Rey, and J. T. Hynes, J. Phys. Chem. A **108**, 1275 (2004).
[62] S. Mukamel, *Principles of Nonlinear Optical Spectroscopy* (Oxford University Press, New York, 1995).
[63] Y.-S. Lin, P. A. Pieniazek, M. Yang, and J. L. Skinner, J. Chem. Phys. **132**, 174505 (2010).
[64] S. T. Roberts, J. J. Loparo, and A. Tokmakoff, J. Chem. Phys. **125**, 084502 (2006).
[65] M. Cho, *Two-Dimensional Optical Spectroscopy* (CRC Press, Boca Raton, 2009).
[66] E. J. Heilweil, F. E. Doany, R. Moore, and R. M. Hochstrasser, J. Chem. Phys. **76**, 5632 (1982).
[67] J. R. Schmidt, S. T. Roberts, J. J. Loparo, A. Tokmakoff, M. D. Fayer, and J. L. Skinner, Chem. Phys. **341**, 143 (2007).
[68] P. Hamm, M. Lim, and R. M. Hochstrasser, Phys. Rev. Lett. **81**, 5326 (1998).
[69] S. Li, J. R. Schmidt, A. Piryatinski, C. P. Lawrence, and J. L. Skinner, J. Phys. Chem. B **110**, 18933 (2006).
[70] C. P. Lawrence and J. L. Skinner, Chem. Phys. Lett. **369**, 472 (2003).
[71] R. G. Gordon, J. Chem. Phys. **44**, 1830 (1966).
[72] E. N. Ivanov, Sov. Phys. JETP **18**, 1041 (1964).
[73] D. Laage and J. T. Hynes, Proc. Natl. Acad. Sci. U.S.A. **104**, 11167 (2007).
[74] S. Li, J. R. Schmidt, S. A. Corcelli, C. P. Lawrence, and J. L. Skinner, J. Chem. Phys. **124**, 204110 (2006).
[75] G. Stock, Phys. Rev. Lett. **102**, 118301 (2009).
[76] J. L. Skinner, Theor. Chem. Acc. **128**, 147 (2011).
[77] C. P. Lawrence and J. L. Skinner, Proc. Natl. Acad. Sci. U.S.A. **102**, 6720 (2005).
[78] C. P. Lawrence, A. Nakayama, N. Makri, and J. L. Skinner, J. Chem. Phys. **120**, 6621 (2004).